ORIGINAL RESEARCH ARTICLE



Minimal Physiologically-Based Pharmacokinetic Modeling of Atenolol and Metoprolol Absorption in Malnourished Rats

Fatma Kir^{1,2} · Selma Sahin¹ · William J. Jusko²

Accepted: 9 March 2025 / Published online: 2 April 2025 © The Author(s) 2025

Abstract

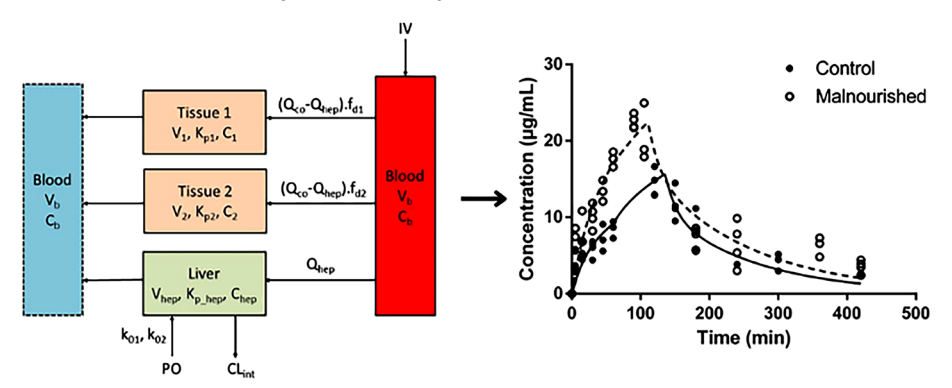
Background and Objective The pharmacokinetics of drugs can be altered by pathophysiological changes in the body that result from malnutrition. The objective of this study was to evaluate the profiles derived from in vivo studies conducted on non-malnourished (control) and malnourished rats using minimal physiologically based pharmacokinetic (mPBPK) models. **Methods** Single oral doses of atenolol (ATN) and metoprolol (MET) were administered to non-malnourished and malnourished rats. We demonstrate how plasma profiles can be evaluated using mPBPK models with high and low tissue-to-plasma partition coefficients (K_p) and elimination by either kidney or liver. A decrease in blood flow and cardiac output due to betablocker administration was assumed. Reference IV profiles from the literature were included to inform the mPBPK model and to help assess the absorption phases of individual oral profiles. Absorption was captured as two or three sequential zero-order processes for both drugs, and IV and oral profiles were assessed by joint fitting. Modeling was performed using both naïve pooling (ADAPT) and population (Monolix) analyses.

Results The experimental data show increased AUC values of MET and ATN in malnourished rats. Accordingly, an increased bioavailability (from 0.43 to 0.67) for ATN and an increased bioavailability (from 0.42 to 0.84) for MET in the malnourished group were related to higher absorption rates in both absorption phases.

Conclusions This study demonstrated advantageous use of mPBPK modeling with malnutrition primarily altering drug absorption in this animal model. Also, our analysis offers a blend of known and assumed components assembled mechanistically to suggest a reasonable interpretation of the PK profiles.

Graphical Abstract

Minimal Physiologically Based Pharmacokinetic Modeling of Atenolol and Metoprolol Absorption in Malnourished Rats



mPBPK model for Metoprolol

Key Points

Pathophysiological changes in the body resulting from malnutrition can alter drug absorption.

The absorption characteristics of non-malnourished and malnourished rats were compared by minimal physiologically based pharmacokinetic models following atenolol and metoprolol administration.

The enhanced bioavailability of atenolol and metoprolol in malnourished rats was attributed to higher absorption rates.

1 Introduction

Malnutrition is defined as a pathological condition resulting from protein and/or calorie deficiency, often associated with infection [1]. Over the last 30 years, the prevalence of malnutrition in hospitalized patients has ranged between 19% and 80% [2]. Malnutrition is seen in developed countries since it can also be caused by diseases such as AIDS, cancer, and anorexia nervosa [3]. Pathophysiological changes (e.g., total intestinal surface area, delayed gastrointestinal emptying time, intestinal transit time, and transporter and enzyme expression) in malnutrition may also affect the absorption and disposition of drugs [4, 5]. For instance, the extent of absorption for caffeine, paracetamol, and chloramphenicol were significantly increased with malnutrition while decreasing for carbamazepine and chloroquine. The plasma protein binding of chloroquine increased, while that of digoxin, streptomycin, and penicillin decreased. Additionally, the clearance of metronidazole, quinine, and isoniazid was decreased in malnutrition [6].

Atenolol (ATN) and metoprolol (MET) are beta-1 adrenergic receptor antagonist drugs used in the treatment of diseases such as hypertension, angina pectoris, and cardiac failure. The solubility of MET and degree of absorption in humans are high ($f_a \ge 85\%$); accordingly, it is classified as a Class I (high solubility, high permeability) compound based on the Biopharmaceutical Classification System (BCS) [7]. Its log P is 1.76 [8]. Following oral administration, MET is completely absorbed from the gastrointestinal tract (GIT). The absorption of MET from the stomach is negligibly low in rats while the absorbed amount is high in the small intestine. In the small intestine, the MET absorption rate in rats (k_a) is 0.66 at pH 6.2 and 0.81 h⁻¹ at pH 7.5, while the

absorption rate of MET in the colon in rats at pH 7.5 is 1.21 h^{-1} ; however, total absorption is negligible in the colon and is higher in the small intestine due to its large surface area [9]. Despite the complete absorption of MET, only 4–60% in rats and 38–60% in humans reaches the systemic circulation because of the extensive first-pass effect [10].

The distribution of MET into tissues is rapid and extensive with highest concentrations in the lung, liver and kidneys, and the distribution volume is greater than actual body weight. Approximately 12% of MET is bound to albumin, while its binding to other plasma proteins is negligible. The concentration of MET in erythrocytes is slightly higher than in plasma. MET is eliminated primarily by the mono-oxygenase system in the liver, and approximately 70% of orally administered MET is metabolized by the CYP2D6 enzyme. A small portion (~ 5%) of an oral or IV dose is excreted unchanged in the urine. Changes in hepatic blood flow significantly affect plasma concentration of MET since it is a high-clearance drug [11, 12].

ATN is a hydrophilic (log P = 0.16) [8], and thus it has difficulty passing through cellular membranes and is incompletely absorbed ($f_a = 50-84\%$) from the intestine in humans. ATN is categorized as Class III (high solubility, low permeability), according to the BCS [7]. The absorption of ATN as a poorly permeable drug is GI site-dependent in rats [13]. Plasma protein binding of ATN is low ($\sim 3\%$) and almost all of ATN is eliminated through the kidneys, while approximately 5% is metabolized in the liver [14].

A study was performed to compare high-dose ATN and MET oral absorption in non-malnourished and malnourished rats and showed higher AUC values in the malnourished rats. The purpose of this report is to demonstrate how minimal physiologically-based pharmacokinetic (mPBPK) models can serve to integrate experimental and literature data to provide mechanistic insights into the absorption and disposition of drugs. These drugs were chosen owing to their differences in permeability, while the rat model was selected because of its ease and common use in malnutrition studies [15, 16].

2 Materials and Methods

2.1 Materials

Atenolol was purchased from Sigma-Aldrich (USA). Metoprolol tartrate was kindly supplied by Novartis Pharma (Turkey). Healthy male Sprague-Dawley (SD) rats (weighing 200–250 g) were purchased from Kobay Experimental Animals Laboratory (Ankara, Turkey). This study was carried out according to the protocol approved by the Ethics

Committee of Kobay Experimental Animals Laboratory, Ankara, Turkey.

2.2 Methods

2.2.1 Treatment Protocol

The rats were maintained in an animal room at a temperature of 20–23 °C with a 12-h/12-h light/dark cycle. After 3–4 days for acclimation, they were divided into two groups (n=4) as control (non-malnourished) and malnourished. Malnutrition was developed by feeding rats with a low protein diet (5% protein) while non-malnourished groups were fed the control diet (20% protein) for 17–20 days. The diets were isocaloric and formulated in a pellet form by Arden Diet Research and Experiment (Ankara, Turkey) according to the literature [15, 16]. All rats were fed *ad libitum* at the same frequency, and water was provided *ad libitum*. The rats were fasted overnight before drug administration. Total cholesterol and serum albumin concentrations were measured before experiments.

ATN and MET doses were 250 and 312 mg/kg, based on pilot studies performed in rats with various doses. ATN was suspended in purified water at a dose of 250 mg/kg, while metoprolol tartrate was dissolved in purified water at a dose of 400 mg/kg (equal to 312 mg/kg MET) and administrated orally by a feeding tube. Blood samples (~ 100 µL) were collected via the tail vein at various sampling points (ATN: 0, 30, 60, 90, 120, 180, 240, 300, 360, 420, 450, and 480 min; MET: 0, 5, 15, 30, 45, 60, 90, 105, 120, 150, 180, 240, 300, 360, and 420 min) into heparinized tubes after drug administration. The plasma samples were separated by centrifugation (5 min at 10,000 rpm) and stored at -20°C until analysis. The plasma samples were prepared for analysis according to Yoon et al [10]. The concentrations of ATN and MET in plasma samples were measured using a validated high-performance liquid chromatography method with modifications [17]. The pharmacokinetic (PK) profiles obtained were analyzed using noncompartmental analysis (NCA) and pharmacometric modeling.

The plasma profiles following IV administration of ATN and MET were taken from the literature as references for the oral profiles [10, 18]. The PK of ATN were assessed after an IV dose (1 mg/kg) in male SD rats [18]. MET was given at three different IV doses (0.5, 1, and 2 mg/kg) in male SD rats [10].

Different IV datasets were used for model evaluation by external validation. The PK of ATN was assessed after an IV dose (1.67 mg/kg) in male SD rats, while the PK of R-MET following an IV dose (1.5 mg/kg) was determined in male SD rats [19, 20]. The plasma profile data was digitized using Web Plot Digitizer version 5.0 (Automeris, CA, USA, https://automeris.io).

2.2.2 Model Structure for Atenolol

The mPBPK model with three tissue compartments was used (Fig. 1), Tissue 1 was considered as rapidly perfused, while Tissue 2 as slowly perfused. The tissue-to-plasma partition coefficient (K_p) values for ATN were predicted [21, 22] using GastroPlus PBPK simulator (version 9.9; Simulations Plus, Lancaster, CA, USA). Accordingly, liver, kidney, and lung were defined as Tissue 1 with high K_p values (liver: 2.87, kidney: 3, and lung: 2.63), while the remaining tissues were defined as Tissue 2. ATN is hydrophilic and is excreted mainly by the kidneys. Therefore, the kidney served for elimination.

The following differential equations described the model for ATN in Fig. 1:

$$\begin{split} V_{\text{b}} \cdot R_{\text{b}} \cdot \frac{\text{d}C_{\text{p}}}{\text{d}t} = & \text{Input} + \left(Q_{\text{CO}} - Q_{\text{renal}}\right) \cdot f_{\text{d1}} \cdot R_{\text{b}} \\ & \cdot \left(\frac{C_{1}}{K_{\text{p1}}} - C_{\text{p}}\right) + \left(Q_{\text{CO}} - Q_{\text{renal}}\right) \\ & \cdot f_{\text{d2}} \cdot R_{\text{b}} \cdot \left(\frac{C_{2}}{K_{\text{p2}}} - C_{\text{p}}\right) + Q_{\text{renal}} \\ & \cdot R_{\text{b}} \cdot \left(\frac{C_{\text{renal}}}{K_{\text{p_renal}}} - C_{\text{p}}\right) \end{split}$$

$$C_{\rm p}(0) = 0 \,(\text{PO}), \, C_{\rm p}(0) = \text{dose}/V_{\rm b} \,(\text{IV})$$
 (1)

$$V_1 \cdot \frac{\mathrm{d}C_1}{\mathrm{d}t} = \left(Q_{\mathrm{CO}} - Q_{\mathrm{renal}}\right) \cdot f_{\mathrm{d}1} \cdot R_{\mathrm{b}} \cdot \left(C_{\mathrm{p}} - \frac{C_1}{K_{\mathrm{p}1}}\right) \quad C_1(0) = 0$$
(2)

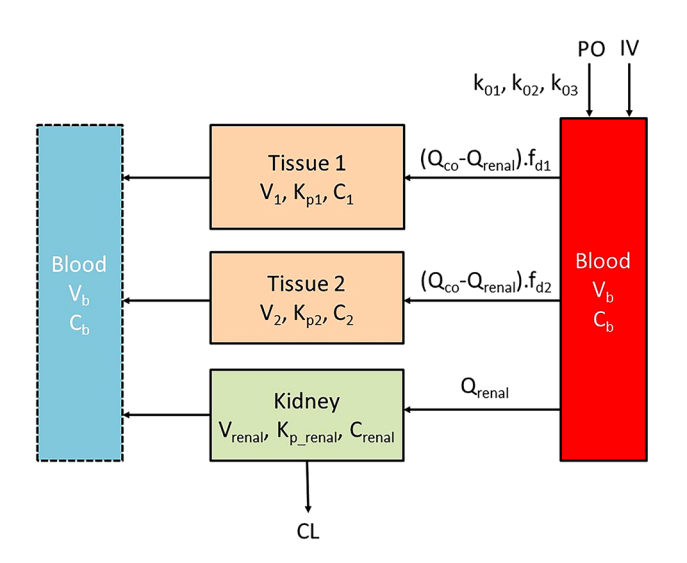


Fig. 1 The minimal physiologically-based pharmacokinetic model extended with the kidneys for ATN. *Symbols* are defined in Tables 2 and S3

$$V_{2} \cdot \frac{dC_{2}}{dt} = \left(Q_{CO} - Q_{renal}\right) \cdot f_{d2} \cdot R_{b} \cdot \left(C_{p} - \frac{C_{2}}{K_{p2}}\right) \quad C_{2}(0) = 0 \qquad V_{2} \cdot \frac{dC_{2}}{dt} = \left(Q_{CO} - Q_{hep}\right) \cdot f_{d2} \cdot R_{b} \cdot \left(C_{p} - \frac{C_{2}}{K_{p2}}\right) \quad C_{2}(0) = 0$$
(7)

$$V_{\text{renal}} \cdot \frac{dC_{\text{renal}}}{dt} = Q_{\text{renal}} \cdot R_{\text{b}} \cdot \left(C_{\text{p}} - \frac{C_{\text{renal}}}{K_{\text{p_renal}}} \right)$$

$$- \text{CL} \cdot C_{\text{p}} \quad C_{\text{renal}}(0) = 0$$
(4)

where C_p is the plasma drug concentration, C_1 , C_2 , C_{renal} are drug concentrations in Tissues 1, 2, and kidney, V_h is the volume of blood, V_1 and V_2 are the volumes of Tissues 1 and 2, $V_{\rm renal}$ is the volume of the kidney, $Q_{\rm co}$ is cardiac output, $f_{\rm d1}$ and $f_{\rm d2}$ are fractions of $Q_{\rm co}$ for Tissues 1 and 2, $Q_{\rm renal}$ is renal blood flow, K_{p1} and K_{p2} are the tissue-to-plasma partition coefficients for Tissues 1 and 2, K_{p_renal} is the tissue-toplasma partition coefficient for kidney, CL is the systemic (renal) clearance, k_{01} , k_{02} , and k_{03} are the apparent zero-order absorption rate constants over designated sequential time intervals, and R_b is the blood-to-plasma ratio.

2.2.3 Model Structure for Metoprolol

MET is lipophilic (log P = 1.76) [8] and is extracted mainly by the liver. Also, the first-pass effect of MET is high, approximately 50% of an oral dose [7, 11]. Therefore, the liver served as the elimination compartment. The kidney, and lung were defined as Tissue 1 with high K_p values (kidney: 14 and lung: 21.15), while the remaining tissues were defined as Tissue 2.

The following differential equations defined the model for MET in Fig. 2:

$$\begin{aligned} V_{\text{b}} \cdot R_{\text{b}} \cdot \frac{\text{d}C_{\text{p}}}{\text{d}t} &= \text{Input IV} + \left(Q_{\text{CO}} - Q_{\text{hep}}\right) \\ & \cdot f_{\text{d1}} \cdot R_{\text{b}} \cdot \left(\frac{C_{1}}{K_{\text{p1}}} - C_{\text{p}}\right) \\ & + \left(Q_{\text{CO}} - Q_{\text{hep}}\right) \cdot f_{\text{d2}} \\ & \cdot R_{\text{b}} \cdot \left(\frac{C_{2}}{K_{\text{p2}}} - C_{\text{p}}\right) + Q_{\text{hep}} \\ & \cdot R_{\text{b}} \cdot \left(\frac{C_{\text{hep}}}{K_{\text{p_hep}}} - C_{\text{p}}\right) \end{aligned}$$

$$C_{\rm p}(0) = 0 \,(\text{PO}), \, C_{\rm p}(0) = \text{dose/V}_{\rm b}(\text{IV})$$
 (5)

$$V_{1} \cdot \frac{\mathrm{d}C_{1}}{\mathrm{d}t} = \left(Q_{\mathrm{CO}} - Q_{\mathrm{hep}}\right) \cdot f_{\mathrm{d}1} \cdot R_{\mathrm{b}} \cdot \left(C_{\mathrm{p}} - \frac{C_{1}}{K_{\mathrm{p}1}}\right) \quad C_{1}(0) = 0 \tag{6}$$

$$V_2 \cdot \frac{dC_2}{dt} = (Q_{CO} - Q_{hep}) \cdot f_{d2} \cdot R_b \cdot \left(C_p - \frac{C_2}{K_{p2}}\right) \quad C_2(0) = 0$$
(7)

(4)
$$V_{\text{hep}} \cdot \frac{dC_{\text{hep}}}{dt} = \text{Input PO} + Q_{\text{hep}} \cdot R_{\text{b}} \cdot \left(C_{\text{p}} - \frac{C_{\text{hep}}}{K_{\text{p_{hep}}}}\right)$$

$$- CL_{\text{int}} \cdot R_{\text{b}} \cdot \frac{C_{\text{hep}}}{K_{\text{p_{hep}}}} \quad C_{\text{hep}}(0) = 0$$
(8)

where V_{hep} is the volume of the liver, Q_{hep} is hepatic blood flow, K_{p1} and K_{p2} are the tissue-to-plasma partition coefficients for Tissues 1 and 2, K_{p_hep} is the tissue-to-plasma partition coefficient for the liver (62.25), and CL_{int} is the intrinsic clearance in liver (C_{hep}) . Other symbols represent the same parameters as in Fig. 1.

The mPBPK models have been based on physiological and anatomical properties by defining the system parameters such as tissue volume, cardiac output, and tissue blood flow rates [23]. Although a change in blood flow in malnutrition was not known to be significant, the decrease in cardiac output and blood flow to the tissues owing to effects of beta blockers was included [24].

The tissue volumes were calculated using:

Body weight =
$$V_b + V_1 + V_2 + V_3$$
 (9)

where V_3 is the kidney or liver volume for ATN or MET [23, 25]. All tissue volumes were fixed to physiological values [26, 27].

Permeability-limited distribution characterized by low f_{d1} and f_{d2} was assumed for ATN [28] as:

$$f_{\rm d,total} = f_{\rm d1} + f_{\rm d2} \le 1 \tag{10}$$

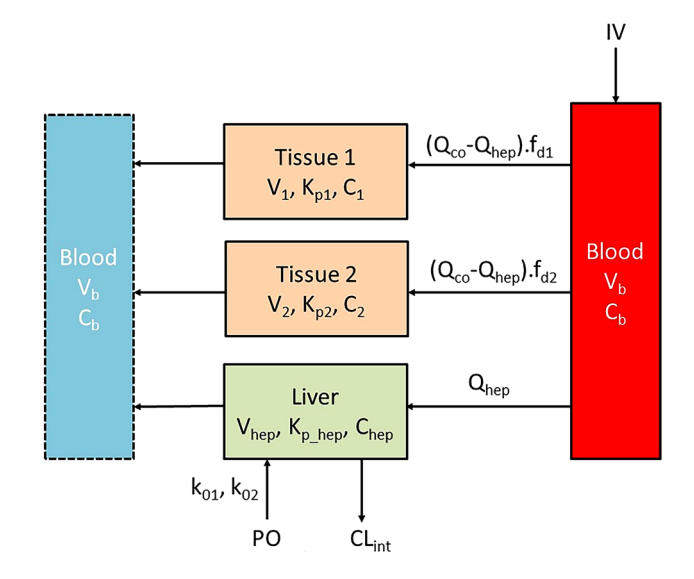


Fig. 2 The minimal physiologically-based pharmacokinetic model extended with the liver for MET. Symbols are defined in Tables 3 and S4

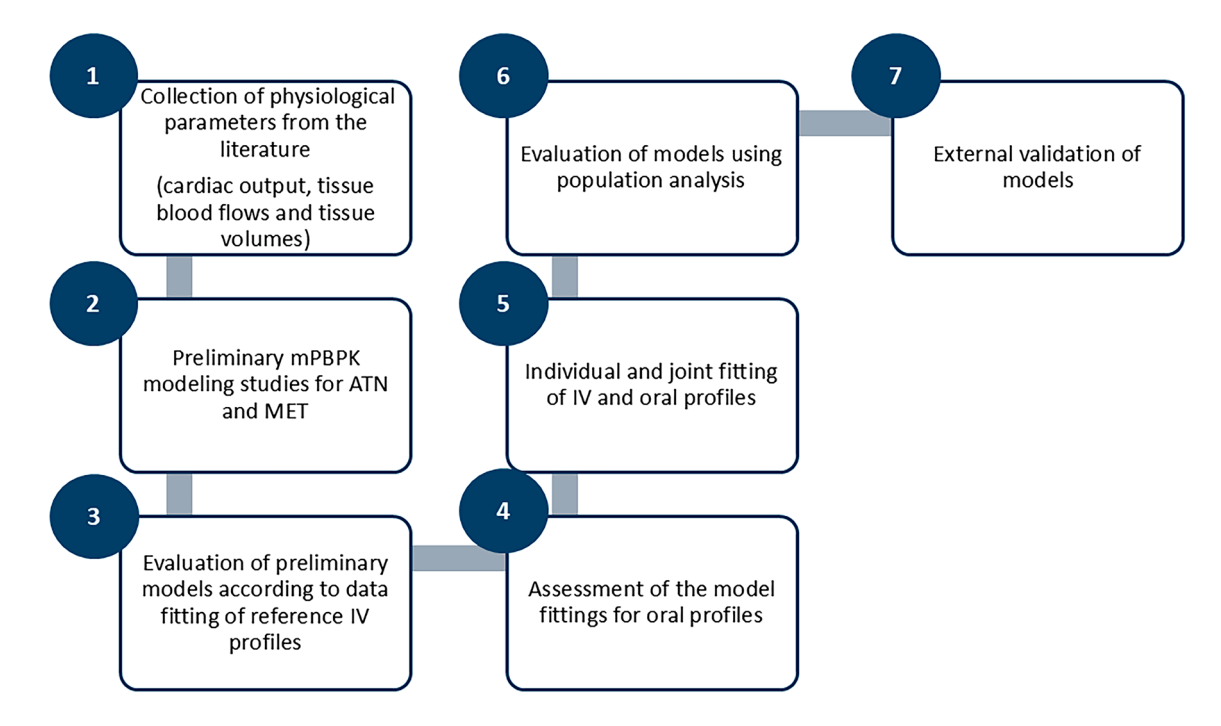


Fig. 3 Flowchart of the modeling process

Perfusion-limited distribution was assumed for MET [28] as:

$$f_{d,total} = f_{d1} + f_{d2} = 1 \tag{11}$$

The R_b value was used to calculate blood concentration-dependent PK parameters using data based on plasma concentrations. The following equation was used to calculate the R_b value [29]:

$$\rho = \frac{\text{HCT} - 1 + R_{\text{b}}}{\text{HCT} \cdot f_{\text{u}}} \tag{12}$$

where ρ is the affinity for blood cells, HCT is the hematocrit, and $f_{\rm u}$ the fraction of drug unbound in plasma.

The ρ value was fixed at 2.57 for MET while it was calculated for ATN. It was reported that the hematocrit (HCT) may change depending on the protein content in diets. Accordingly, the HCT of malnourished and control SD rats were 45.5% and 47.5% [30]. ATN and MET have low plasma protein binding and are primarily bound to albumin. Therefore, $f_{\rm u}$ values for the malnourished group were calculated ($f_{\rm u \ ATN}$: 1.00, $f_{\rm u \ MET}$: 0.908) by comparison to the albumin concentration of the control group ($f_{\rm u \ ATN}$: 0.970, $f_{\rm u \ MET}$: 0.805) [8, 29]. The $R_{\rm b}$ values of ATN for the control and malnourished groups were 1.00 and 1.014, while the $R_{\rm b}$ values of MET were 1.508 and 1.607. Also, the $R_{\rm b}$ value was 1.7 (average of R- and S-MET) for the reference IV administration of MET. Where available, specific $K_{\rm p}$ values were

taken from literature sources rather than being fitted as is typical with mPBPK models.

The estimated $f_{\rm dl}$, $K_{\rm pl}$ and F parameters were dimensionless.

The individual fittings of the data were first tested to ensure the accuracy of the initial parameters and model fitting. Then, all the data (IV and oral) were jointly fitted with most parameters shared for each drug through naïve pooling. Subsequently, population analyses were conducted to simulate broader trends. The results of these analyses were then evaluated to gain insights into the overall patterns and behaviors observed in the data. Figure 3 provides a summary of the steps involved in the modeling process.

2.2.4 Individual Oral Fittings

ATN and MET absorption profiles were first evaluated using a point–area deconvolution method [31]. In this regard, the absorption rate of the drugs at each time point was calculated by comparing IV and PO profiles using:

Input rate =
$$\frac{D_0 \cdot C_{\text{pf}}}{F \cdot \text{AUC}_{\text{IV}}^{(0-t)}}$$
(13)

where D_0 is the dose, $C_{\rm pt}$ is the plasma drug concentration after oral administration at time t, F is the bioavailability, and ${\rm AUC_{\rm rv}}^{(0-t)}$ is the area under the curve at time t for IV administration.

Table 1 Effects of low protein diet on weight, albumin and total cholesterol

Parameter	ATN		MET		
	Control	Malnourished	Control	Malnourished	
Body weight (g)	300 (18.27)	216* (14.99)	302 (16.47)	233** (14.25)	
Serum albumin (g/dL)	4.40 (0.07)	3.75** (0.17)	4.68 (0.13)	4.15** (0.15)	
Total cholesterol (mg/dL)	78.4 (15.01)	50.3** (8.34)	66.5 (10.01)	49.5** (2.69)	

Values are reported as mean (standard deviation)

The results showed that the absorption rates of ATN and MET were relatively constant over differing time frames as an indication of zero-order input [31]. Since two or three phases for each drug were seen, absorption was defined as two or three zero-order processes. The starting and finishing times of these phases were identified in the deconvolution assessment and then optimized by trial and error in the full model fitting process

The apparent bioavailability of each drug was calculated from the dose-normalized total AUC values of the model-fitted oral versus IV plasma concentration profiles.

2.2.5 External Validation

The external validation of the models involved comparison of model predictions with reference IV profiles for different data sets of ATN and MET from the literature [19, 20]. Simulations were performed by fixing estimated parameters for each model and drug and superimposing them on the separate profiles.

2.2.6 Naïve Pooling

Naïve pooled data included IV and oral profiles of all rats. In reference IV profiles, the standard deviations for each point were also digitized and assumed as different rats. Thus, three rats were evaluated for each IV reference dose. The naïve pooling involved fitting of all IV and PO data jointly.

2.2.7 Population Analysis (PopPK)

The PK parameters from the IV references were fitted using the mPBPK models. The estimated parameters ($f_{\rm dl}$, $K_{\rm pl}$, and CL) were fixed in the control and malnourished groups for assessment of absorption profiles (a two-stage analysis). Between-subject variability (ω^2) of the parameters and the random effects were assumed to be log-normally distributed. Various error models (e.g., constant, proportional, and combined) were applied to define residual errors. The proportional error model was used for all groups, while the constant error model was used to define MET oral profiles. The linearization method was used to calculate the Fisher

Information Matrix, and standard errors of the parameters were estimated. According to the evaluations, the random effect of CL was included in the model for both drugs.

The relationship for observation Y_{ij} is described for the *j*th observed concentration of the *I*th individual using:

$$\log(Y_{ii}) = \log(c_{\text{pred},ii}) + b.\log(c_{\text{pred},ii}).\varepsilon_{ii}$$
 (14)

where $c_{\text{pred},ij}$ is the estimated drug concentration for the *j*th concentration of the *i*th individual, *b* is the proportional error term, and ε_{ij} is assumed to be a standardized Gaussian random variables representing residual error for the *j*th concentration of the *i*th individual, with zero as a mean and a variance of σ_2 [32].

The models were evaluated by visual inspection of diagnostic plots, -2 times log-likelihood (-2LL), Akaike Information Criterion (AIC), Bayesian Information Criteria (BIC), Corrected Bayesian Information Criteria (BICc), and the relative standard errors of the parameter estimates (RSE).

Statistical comparisons were conducted with the Kruskal–Wallis test followed by Mann–Whitney *U* as a post hoc analysis with IBM SPSS (version 29.0). NCA was conducted using PKanalix (version 2023 R1; Lixoft, Antony, France). The naïve pooled analysis was performed using ADAPT 5 (Biomedical Simulations Resource, Los Angeles, 2009) [33]; and the results were visualized using GraphPad Prism (version 6). Population PK analysis was performed using Monolix (version 2023 R1, Lixoft). The ADAPT and Monolix codes for the IV/oral models of ATN and MET are provided in the Supplementary Materials.

3 Results

Table 1 provides the biochemical measures in the two animal groups after 17–20 days of the two diets. The body weight, serum albumin, and total cholesterol values were significantly reduced in the malnourished groups. These reductions indicate that malnutrition developed in rats fed low protein with changes in concordance with published observations [34]. NCA results are summarized in Supplementary

^{*}p < 0.05 and **p < 0.001 represent significant differences between control and malnourished rats

Table 1. Assessment of these measures as covariates did not improve the population modeling.

3.1 Model Fittings

ATN exhibited a rapid initial decline phase followed by a long linear terminal phase after IV administration. Following oral dosing in the control and malnourished groups, a rapid increase in drug concentration was observed at the first time point. Also, after 120 min, it was observed that the absorption rate increased. The plasma concentrations rose in two apparent phases reaching a similar $C_{\rm max}$ of 25.0 ± 3.82 µg/mL for control and 22.8 ± 2.56 µg/mL for malnourished groups at 240–300 min. The plasma drug concentrations then showed a rapid decay after $t_{\rm max}$ in the controls which was similar to the IV data, while a differing slow decay was seen in the malnourished group. These behaviors plus the preliminary deconvolution analysis led to our assumption that ATN has 2 or 3 absorption phases.

Physiological parameters of tissues used for the mPBPK models are shown in Supplementary Table S2. The population and jointly fitted IV and oral (control and malnourished) data of ATN are shown in Figs. 4 and S1.

The final PopPK parameter estimates of ATN are summarized in Tables 2 and S3. The disposition-related parameters $(f_{d1}, K_{p1}, \text{ and CL})$ were shared in all groups. The f_{d1} and $f_{\rm d2}$ were assumed to be equal and found to be very small (0.134), which is consistent with the low permeability of ATN (Table 2). In the PopPK, k_{01} and k_{02} were evaluated separately, and there was no significant difference between the control and malnourished groups $(k_{01} C \text{ vs } k_{01} M, k_{02}$ C vs k_{02} M). Therefore, k_{01} and k_{02} were shared in the joint fitting. The t_{max} was fixed at 300 min for both control and malnourished groups according to visual inspection. The duration of the first absorption phase (t_1) was determined based on deconvolution and trial and error, and then fixed to 120 min for both groups. Consequently, the difference between the control and malnourished groups may be due to absorption in the third phase (k_{03}) .

MET also exhibited apparent IV biexponential disposition kinetics. The PK data for three IV dose levels showed linearity. Following oral administration, MET showed a rapid increase in drug concentration at initial time points for both groups. The absorption rate increased after 60 min for the control group, while it appeared similar throughout the entire absorption phase for the malnourished group. After $t_{\rm max}$, the drug concentration decreased similarly for both groups. The $C_{\rm max}$ at 100-120 min was 14.3 ± 1.54 µg/mL in the control and 20.6 ± 3.12 µg/mL in the malnourished group. The oral decline phases were slower than those from the IV curves.

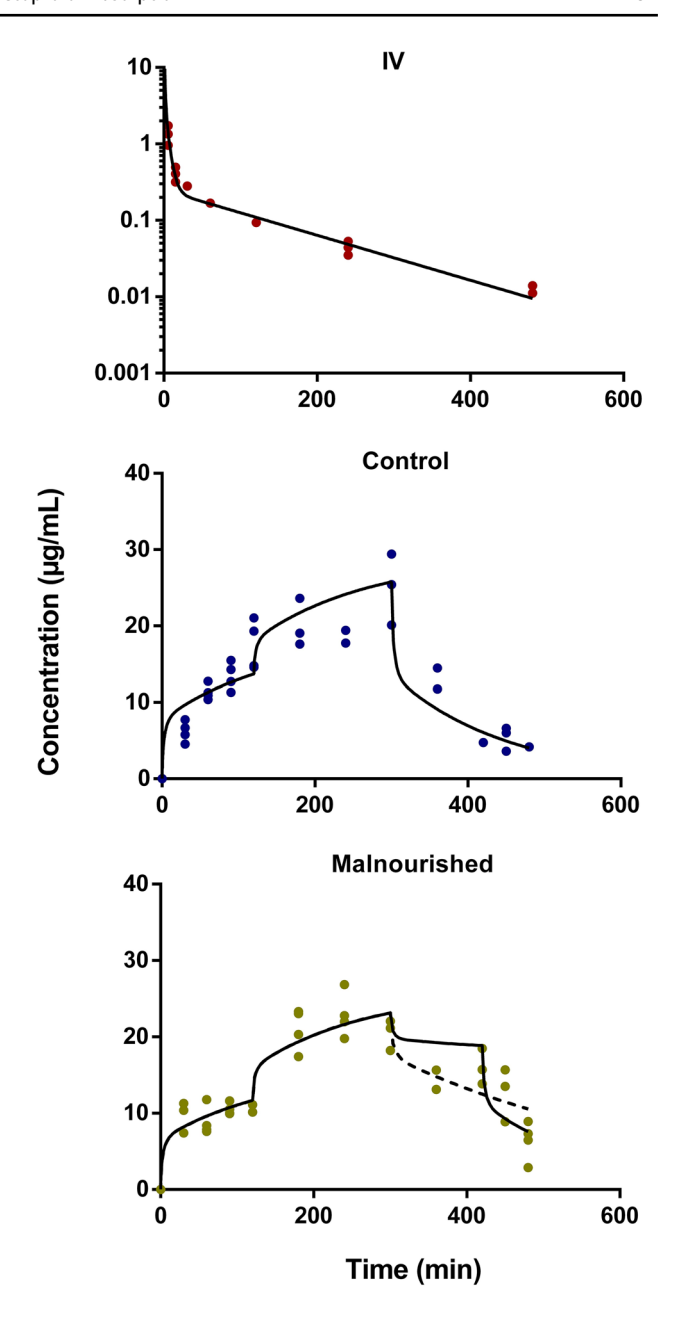


Fig. 4 Population fits for ATN plasma concentrations versus time. *Symbols* are observations and lines are population fittings, while the *dashed line* shows the fitting without k_{03}

Figures 5 and S2 illustrate population and jointly fitted IV and oral data of MET. The final parameter estimates of MET obtained by population and joint fitting are summarized in Tables 3 and S4.

Parameters related to disposition ($f_{\rm d1}$, $K_{\rm p2}$ and CL) were shared in all groups. The $f_{\rm d1}$ (0.464) and $f_{\rm d2}$ (0.536) for MET were higher than for ATN (Table 3). This is in accordance with the perfusion-limited assumption for MET. The absorption phases were defined separately for the control and malnourished groups. The absorption rate constants were not

Table 2 Estimated population pharmacokinetic parameters for atenolol

Parameter	Definition	Value	Linearization	
			SE	RSE (%
Fixed effects				
$f_{\rm d1}^{\ a}$	Fractional distribution parameter for Tissue 1	0.134	0.016	11.9
K_{p1}^{b}	Tissue-to-plasma partition coefficient for Tissue 1	1.43	0.0973	6.81
CL (mL/min/kg)	Total clearance	16.04	1.28	8.00
$k_{01} C \text{ (mg/min/kg)}$	Apparent zero-order absorption rate constant 1 ($t = 0$ –120 min)	1.19	0.0758	6.38
$k_{01} M \text{ (mg/min/kg)}$		1.012*	0.0633	6.26
$k_{02} C \text{ (mg/min/kg)}$	Apparent zero-order absorption rate constant 2 ($t = 120-300 \text{ min}$)	1.86**	0.138	7.41
$k_{02} M \text{ (mg/min/kg)}$		1.68	0.134	7.99
$k_{03} C^{c}$ (mg/min/kg)	Apparent zero-order absorption rate constant 3 ($t = 300-360 \text{ min}$)	0		
$k_{03} M \text{ (mg/min/kg)}$	Apparent zero-order absorption rate constant 3 ($t = 300-420 \text{ min}$)	1.16	0.147	12.6
V _{ss} (L/kg) ^d	Volume of distribution at steady-state	1.41		
F C ^e	Apparent absolute bioavailability	0.426		
FM^{e}		0.673		
Standard deviation of t	he random effects			
		Value (CV%)		
ω CL	Random effect of CL	0.124 (12.5)	0.0589	47.4
Error model parameter	3			
b IV	Proportional error term	0.154	0.0328	21.3
b C		0.256	0.03204	12.5
b M		0.234	0.0272	11.6

RSE relative standard error, SE estimated standard error

shared in the joint fitting and were evaluated as separate parameters to compare the two groups. The t_{max} was fixed at 135 and 110 min for the control and malnourished groups, respectively, and t_1 was fixed to 60 min for both groups by optimization. Since k_{0I} values have units of amount/time (mg/min/kg), the overall bioavailability (F) was calculated using the predicted concentration versus time profiles from $F = AUC_{PO}/AUC_{IV}$. Consistent with the parameters and observed higher concentrations in the malnourished groups, F increased from 0.43 to 0.67 for ATN and from 0.42 to 0.84 for MET. The population models were optimized by using 0.34 and 0.27 fractions of the CL obtained from the IV fitting for control and malnourished groups according to goodness of fit (GoF). Thus, the CL value for the oral profiles $(43.8 \pm 5.92 \text{ mL/min/kg})$ was found similar to the CL estimated in the joint fitting (40.4 mL/min/kg).

3.2 Population metrics

Profiles for population fittings are shown in Figs. 4 and 5. Reference IV and oral (control and malnutrition groups) profiles were well predicted by the mPBPK model. Also, model predictions describing absorption phases as two or three zero-order processes for the malnourished group are shown in Tables 2 and 3, respectively. The outlier proportions for observations and predictions for ATN and MET were found to be $7.59 \pm 0.52\%$ and $10.32 \pm 2.26\%$, respectively. Scatter plots of the residuals had no pattern or trend. Visual predictive check plots are shown in Figures S3 and S4. Estimated population parameters for ATN and MET are listed in Tables 2 and 3, respectively. All the parameters were estimated well since they have low SE and RSE% values.

 $^{{}^{}a}f_{d1} = f_{d2}$

 $^{{}^{\}rm b}K_{\rm p1} = K_{\rm p2}$

^cAssumed to be 0 according to GoF

^dCalculated based on $V_{ss} = (V_b + V_1 \cdot K_{p1} + V_2 \cdot K_{p2} + V_3 \cdot K_{p3})$ /body weight

^eCalculated based on $F = (AUC_{PO} \cdot Dose_{IV})/(AUC_{IV} \cdot Dose_{PO})$, C: control group, M: malnourished group

^{*}Significantly lower than k_{02} C and k_{02} M (p < 0.05)

^{**}Significantly higher than $k_{03} M (p < 0.05)$

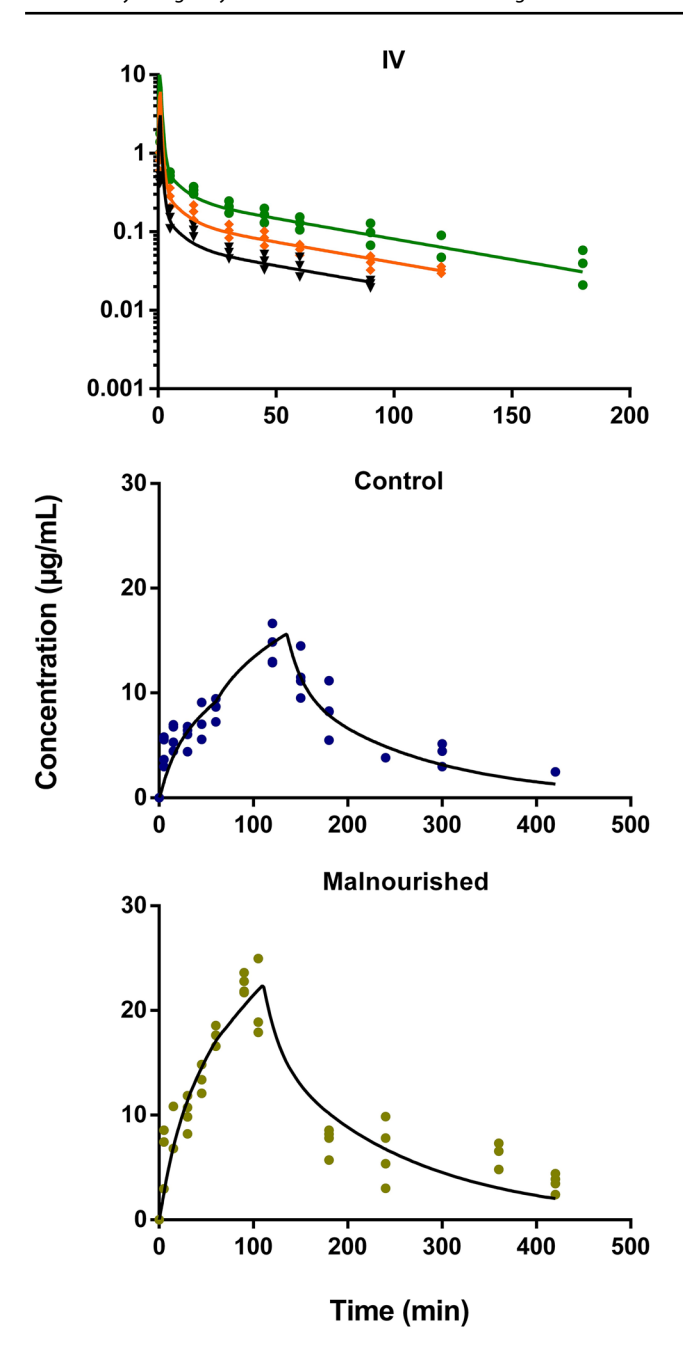


Fig. 5 Population fits for MET plasma concentrations versus time. *Symbols* are observations and *lines* are population fittings

3.3 External Validation of the Models

Simulation studies were performed comparing separate sources of PK data, as shown in Fig. 6. Although the published data for ATN are not as conclusive as MET, they were well-captured by ADAPT and Monolix.

The MET data was predicted well by Monolix, while only the early data were captured by ADAPT. This may be related to the different factors (e.g., the random effect of CL)

considered for popPK analysis, while the error model terms used in ADAPT 5 and Monolix differ.

Our $K_{\rm p_hep}$ was calculated assuming mixed R- and S-isomers of the MET IV reference; however, the external dataset used for MET was obtained after R-MET administration. Therefore, the $K_{\rm p_hep}$ was fixed to 39.1 as a closed-loop $K_{\rm p}$ estimation of R-MET [19]. The late overestimation may be related to the stereoselective metabolism of MET as R-MET has a 40% higher clearance than S-MET due to metabolism by the CYP2D6 enzyme in humans [35]. In any case, there is consistency in the PK with our studies, adding credibility to the assessment of ATN and MET absorption.

4 Discussion

ATN and MET have been given orally to rats in several studies. Yoon et al. administered MET orally to healthy male SD rats (200–250 g) at doses of 1, 2, and 5 mg/kg, and evaluated the PK [10]. ATN was given orally to healthy male Wistar rats at doses of 1 mg/kg [36]. However, in most of the studies, PK parameters were evaluated by NCA. The PK profiles of ATN and MET in malnourished rats have not been assessed.

Both increased and decreased absorption, protein binding, distribution volumes, and clearances have been observed in malnutrition, as reviewed by [4]. The changes appear to be drug-specific. There have been few modeling studies to examine the changes in the PK of drugs during malnutrition. Linear mammillary plasma clearance models were used for the PK evaluation of ketamine in malnourished rats [16], and it was concluded that the absorption rate was increased and clearance was decreased during malnutrition. Ketamine is primarily metabolized by CYP450 enzymes (CYP2B6, 2C9, and 3A4) and undergoes extensive first-pass metabolism. Body composition differences between healthy and malnourished adults and children were assessed [37], and the decrease in organ components was defined according to malnutrition levels, and physiological scaling parameters for the translation of physiological changes at different levels of malnutrition were identified. Thus, virtual malnourished pediatric populations were created and a PBPK model was proposed accordingly. Alterations in drug exposure (increase for caffeine, cefoxitin, and ciprofloxacin; decrease for lumefantrine, pyrimethamine, and sulfadoxine) were attributed to changes in elimination capacity in malnutrition.

Our study assessed the PK of ATN and MET for control and malnourished rats after oral dosing to demonstrate the advantages of mPBPK modeling. The mPBPK models include anatomical and physiological components and can successfully define plasma PK profiles of drugs when only blood/plasma data are available. Also, mPBPK models are flexible since they involve a 'lumping' approach by

Table 3 Estimated population pharmacokinetic parameters for metoprolol

Parameter	Definition	Value	Linearization	
			SE	RSE (%)
Fixed effects				
f_{d1}^{a}	Fractional distribution parameter for Tissue 1	0.464	0.104	22.4
K_{p1}	Tissue-to-plasma partition coefficient for Tissue 1	4.033	0.54	13.4
CL _{int} (mL/min/kg)	Intrinsic clearance	148	26.7	18.0
$k_{01} C \text{ (mg/min/kg)}$	Apparent zero-order absorption rate constant 1 ($t = 0$ –60 min)	4.5*	0.463	10.3
$k_{01} M \text{ (mg/min/kg)}$		7.56	0.611	8.076
$k_{02} C \text{ (mg/min/kg)}$	Apparent zero-order absorption rate constant 2 ($t = 60-135 \text{ min}$)	5.57	1.02	18.4
$k_{02} M \text{ (mg/min/kg)}$	Apparent zero-order absorption rate constant 2 ($t = 60-110 \text{ min}$)	7.12	1.12	15.8
fr C	Fraction of CL _{int}	0.336	0.0611	18.2
fr M		0.256	0.0387	15.1
$V_{\rm ss}$ (L/kg)	Volume of distribution at steady-state	5.82		
FC	Apparent absolute bioavailability	0.422		
FM		0.839		

Standard deviation of the random effects

		Value	CV%		
ωCL	Random effect of total clearance	0.258	26.2	0.137	53.2
Error model p	arameters				
b IV	Proportional error term	0.365		0.033	9.11
a C	Constant error term	1.76		0.194	11.04
а М		2.54		0.274	10.78

^{*}Significantly lower than $k_{01} M (p < 0.05)$

RSE relative standard error, SE estimated standard error

combining tissues with similar kinetic properties [23]. The mPBPK model for MET was expanded with the liver and first-pass effect included, while the model for ATN included the kidney. Oral profiles were evaluated by informing the mPBPK model with literature IV data, which included use of same K_p values from literature sources and reducing blood flows in accordance with expected effects of the beta-blockers.

An increased apparent bioavailability (from 0.43 to 0.67) for ATN and an increased bioavailability (from 0.42 to 0.84) for MET in the malnourished group were related to higher absorption rates in both absorption phases. The incomplete F for ATN can be attributed to its low permeability, while the incomplete F for MET may be related to its first-pass effect, as its bioavailability based on Q_h and CL_{int} is expected to be 0.79 (from $F^* = 1 - CL_h/Q_h$ where CL_h is the IV dose/AUC).

The absorption of drugs is well known to vary in different segments of the GIT [38]. The results of in situ studies conducted to investigate the permeability of ATN and MET in different segments of the rat intestine indicated that the

absorption of both drugs varies depending on the region, since the permeability of ATN and MET varies depending on GIT pH [9, 13]. This is consistent with the absorption of ATN and MET exhibiting two or three absorption phases. Similar to our approach, differences in the plasma time-course phases after oral dosing have been interpreted using "finite absorption time" models where site-dependent absorption rates can be evidenced as drugs move down the GIT, even limiting bioavailability [39, 40]. Segmental differences in drug absorption rates are commonly found in commercial software such as GastroPlus (Simulations Plus). The absorption of drugs may increase due to the loosening of tight junctions between cells in malnutrition [5].

The naïve pooling approach assumes that all data are combined and analyzed as if originating from a single subject. This is straightforward and easily implemented. Moreover, incorporating various datasets can potentially enhance the reliability of the estimations. Conversely, while population analyses are inherently more complex than naïve pooling, they facilitate the derivation of more accurate estimates

 $^{^{}a}f_{d2} = 1 - f_{d1}$, symbols and calculations as described in Table 2

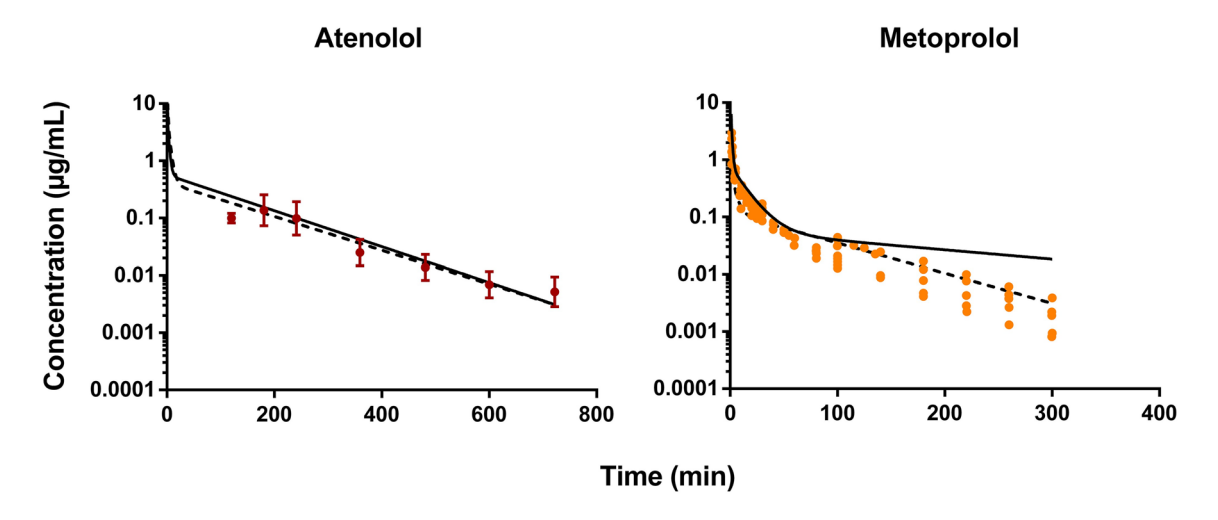


Fig. 6 Simulations for ATN and MET and comparison with external datasets. *Symbols* reflect observations (± 2SD), *solid line* the profile predicted by ADAPT, *dashed line* the profile predicted by Monolix

by incorporating factors such as inter-individual differences and residual intra-individual variability.

The naïve pooling and PopPK assessments, along with optimization (t_I values) and findings, provided reasonable fittings. Similar results were found by naïve pooling and joint fittings in ADAPT, as shown in the Supplementary Materials. Limitations of this study are the study of only two drugs, and that IV profiles of healthy rats came from the literature and were assumed relevant for the oral dose groups. The drug-induced change in blood flows should better be related pharmacodynamically to the concentrations. However, the PK of the study drugs is linear in rats, and the oral and IV plasma concentrations were within a 10-fold range. Further, the physiological parameters of malnourished rats were assumed unchanged relative to body weight affected similarly by the beta-blockers. The possibility of both altered absorption and reduced clearance cannot be ruled out in the malnourished rats, as reduced clearance has sometimes been observed in malnourished humans [4]. Nevertheless, it is quite evident that the time-course profiles differed between the control and malnourished groups consistent with differences in absorption. This is basically a pilot study. More intensive blood and GI sampling using a range of IV and oral doses would be necessary to comprehensively evaluate more mechanistic models.

A particular goal of this study is the demonstration of the integration of experimental and literature data using PopPK methodology for mechanistically relevant mPBPK models. Besides the physiological distribution elimination construct, the model allows for altered blood flow and the input of MET to be influenced by both transient rate GI absorption and possible first-pass through the liver. The PK of ATN

does not involve first-pass, but provides complementary information for a low versus high permeability drug.

5 Conclusions

The experimental data clearly show increased AUC values of MET and ATN in malnourished rats. Our analysis, like with the operation of full PBPK models, offers a blend of known and assumed components assembled mechanistically to offer a reasonable interpretation of the PK profiles.

Supplementary Information The online version contains supplementary material available at https://doi.org/10.1007/s13318-025-00943-6.

Declarations

Conflict of interest All authors declare that they have no conflicts of interest.

Funding This study was funded by Hacettepe University Scientific Research Projects Coordination Unit (TSA-2022-19747), The Scientific and Technological Research Council of Turkey (2211-C and 2214-A) and The National Institute of General Medical Sciences (R35-GM131800).

Ethical approval This study was approved by The Ethics Committee of Kobay Experimental Animals Laboratory Inc, Ankara, Turkey, with protocol number 583 on October 15, 2021.

Consent to participate Not applicable.

Consent for publication Not applicable.

Availability of data and material All data from this study are provided in the figures.

Code availability The modeling code is provided in the Supplementary Materials.

Author contributions Participated in research design: Kir, Sahin, Jusko. Conducted experiments: Kir. Performed data analysis: Kir, Jusko. Wrote or contributed to the writing of the manuscript: Kir, Sahin, Jusko. Supervision, project administration, and funding acquisition: Sahin, Jusko. All authors have read and agreed to the manuscript.

Open Access This article is licensed under a Creative Commons Attribution-NonCommercial 4.0 International License, which permits any non-commercial use, sharing, adaptation, distribution and reproduction in any medium or format, as long as you give appropriate credit to the original author(s) and the source, provide a link to the Creative Commons licence, and indicate if changes were made. The images or other third party material in this article are included in the article's Creative Commons licence, unless indicated otherwise in a credit line to the material. If material is not included in the article's Creative Commons licence and your intended use is not permitted by statutory regulation or exceeds the permitted use, you will need to obtain permission directly from the copyright holder. To view a copy of this licence, visit http://creativecommons.org/licenses/by-nc/4.0/.

References

- Nnakwe N. The effect and causes of protein-energy malnutrition in Nigerian children. Nutr Res. 1995;15(6):785–94. https://doi. org/10.1016/0271-5317(95)00044-J.
- Waitzberg DL, Ravacci G, Raslan M. Desnutrición hospitalaria. Nutr Hosp. 2011;26(2):254–64. https://doi.org/10.3305/nh.2011. 26.2.5070.
- Schaible UE, Kaufmann SHE. Malnutrition and infection: complex mechanisms and global impacts. PLoS Med. 2007;4(5): e115. https://doi.org/10.1371/journal.pmed.0040115.
- Verrest L, Wilthagen EA, Beijnen JH, Huitema AD, Dorlo TP. Influence of malnutrition on the pharmacokinetics of drugs used in the treatment of poverty-related diseases: a systematic review. Clin Pharmacokinet. 2021;60:1149–69. https://doi.org/10.1007/ s40262-021-01031-z.
- Ferraris RP, Carey HV. Intestinal transport during fasting and malnutrition. Annu Rev Nutr. 2000;20(1):195–219. https://doi. org/10.1146/annurev.nutr.20.1.195.
- Oshikoya KA, Sammons HM, Choonara I. A systematic review of pharmacokinetics studies in children with protein-energy malnutrition. Eur J Clin Pharmacol. 2010;66:1025–35. https://doi.org/ 10.1007/s00228-010-0851-0.
- Yang Y, Faustino PJ, Volpe DA, Ellison CD, Lyon RC, Yu LX. Biopharmaceutics classification of selected β-blockers: solubility and permeability class membership. Mol Pharm. 2007;4(4):608– 14. https://doi.org/10.1021/mp070028i.
- Jeong Y-S, Yim C-S, Ryu H-M, Noh C-K, Song Y-K, Chung S-J. Estimation of the minimum permeability coefficient in rats for perfusion-limited tissue distribution in whole-body physiologically-based pharmacokinetics. Eur J Pharm Biopharm. 2017;115:1–17. https://doi.org/10.1016/j.ejpb.2017.01.026.
- Doménech J, Alba M, Morera J, Obach R, Plá DJ. Gastric, intestinal and colonic absorption of metoprolol in the rat. Br J Clin Pharmacol. 1985;19(S2):85S-S89. https://doi.org/10.1111/j.1365-2125.1985.tb02747.x.

- Yoon I-S, Choi M-K, Kim JS, Shim C-K, Chung S-J, Kim D-D. Pharmacokinetics and first-pass elimination of metoprolol in rats: contribution of intestinal first-pass extraction to low bioavailability of metoprolol. Xenobiotica. 2011;41(3):243–51. https://doi.org/10.3109/00498254.2010.538090.
- Regårdh C-G, Johnsson G. Clinical pharmacokinetics of metoprolol. Clin Pharmacokinet. 1980;5(6):557–69. https://doi.org/10. 2165/00003088-198005060-00004.
- Berger B, Bachmann F, Duthaler U, Krähenbühl S, Haschke M. Cytochrome P450 enzymes involved in metoprolol metabolism and use of metoprolol as a CYP2D6 phenotyping probe drug. Front Pharmacol. 2018;9: 395733. https://doi.org/10.3389/fphar. 2018.00774.
- 13. Roos C, Dahlgren D, Sjögren E, Tannergren C, Abrahamsson B, Lennernäs H. Regional intestinal permeability in rats: a comparison of methods. Mol Pharm. 2017;14(12):4252–61. https://doi.org/10.1021/acs.molpharmaceut.7b00279.
- Kirch W, Görg K. Clinical pharmacokinetics of atenolol—a review. Eur J Drug Metab Pharmacokinet. 1982;7:81–91. https://doi.org/10.1007/BF03188723.
- Varma DR. Influence of dietary protein on the anti-inflammatory and ulcerogenic effects and on the pharmacokinetics of phenylbutazone in rats. JPET. 1979;211(2):338–44.
- Williams ML, Mager DE, Parenteau H, Gudi G, Tracy TS, Mulheran M, et al. Effects of protein calorie malnutrition on the pharmacokinetics of ketamine in rats. DMD. 2004;32(8):786–93. https://doi.org/10.1124/dmd.32.8.786.
- Kir F, Dogan A, Sahin S. Development of a RP-HPLC method for simultaneous determination of atenolol, metoprolol tartrate and phenol red for in-situ rat intestinal perfusion studies. J Chromatogr B. 2024. https://doi.org/10.1016/j.jchromb.2024.124160.
- Kumar S, Ravulapalli SY, Tiwari SK, Gupta S, Nair AB, Jacob S. Effect of sex and food on the pharmacokinetics of different classes of BCS drugs in rats after cassette administration. Int J Pharm. 2021;610: 121221. https://doi.org/10.1016/j.ijpharm.2021. 121221.
- Cheung S, Rodgers T, Aarons L, Gueorguieva I, Dickinson G, Murby S, et al. Whole body physiologically based modelling of β-blockers in the rat: events in tissues and plasma following an iv bolus dose. Br J Pharmacol. 2018;175(1):67–83. https://doi.org/ 10.1111/bph.14071.
- Ni J, Ouyang H, Aiello M, Seto C, Borbridge L, Sakuma T, et al. Microdosing assessment to evaluate pharmacokinetics and drug metabolism in rats using liquid chromatography-tandem mass spectrometry. Pharm Res. 2008;25:1572–82. https://doi.org/10. 1007/s11095-008-9555-x.
- Rodgers T, Leahy D, Rowland M. Physiologically based pharmacokinetic modeling 1: predicting the tissue distribution of moderate-to-strong bases. J Pharm Sci. 2005;94(6):1259–76. https:// doi.org/10.1002/jps.20322.
- Rodgers T, Rowland M. Physiologically based pharmacokinetic modelling 2: predicting the tissue distribution of acids, very weak bases, neutrals and zwitterions. J Pharm Sci. 2006;95(6):1238–57. https://doi.org/10.1002/jps.20502.
- Cao Y, Jusko WJ. Applications of minimal physiologically-based pharmacokinetic models. J Pharmacokinet Pharmacodyn. 2012;39:711–23. https://doi.org/10.1007/s10928-012-9280-2.
- Risberg J, Hordnes C, Tyssebotn I. The effect of β1-adrenoceptor blockade on cardiac output and organ blood flow in conscious rats. Scand J Clin Lab Investig. 1987;47(6):521–7. https://doi.org/10. 1080/00365518709168463.
- Li X, Jusko WJ. Utility of minimal physiologically based pharmacokinetic models for assessing fractional distribution, oral absorption, and series-compartment models of hepatic clearance. DMD. 2023;51(10):1403–18. https://doi.org/10.1124/dmd.123.001403.

- Shah DK, Betts AM. Towards a platform PBPK model to characterize the plasma and tissue disposition of monoclonal antibodies in preclinical species and human. J Pharmacokinet Pharmacodyn. 2012;39:67–86. https://doi.org/10.1007/s10928-011-9232-2.
- Li X, DuBois DC, Almon RR, Jusko WJ. Physiologically based pharmacokinetic modeling involving nonlinear plasma and tissue binding: application to prednisolone and prednisone in rats. JPET. 2020;375(2):385–96. https://doi.org/10.1124/jpet.120.000191.
- Jeong Y-S, Jusko WJ. Meta-assessment of metformin absorption and disposition pharmacokinetics in nine species. Pharmaceuticals. 2021;14(6):545. https://doi.org/10.3390/ph14060545.
- Rodgers T, Leahy D, Rowland M. Tissue distribution of basic drugs: accounting for enantiomeric, compound and regional differences amongst β-blocking drugs in rat. J Pharm Sci. 2005;94(6):1237–48. https://doi.org/10.1002/jps.20323.
- 30. Edozien JC, Switzer BR. Effects of dietary protein, fat and energy on blood hemoglobin and hematocrit in the rat. J Nutr. 1977;107(6):1016–21. https://doi.org/10.1093/jn/107.6.1016.
- Cheng H, Jusko WJ. The area function method for assessing the drug absorption rate in linear systems with zero-order input. Pharm Res. 1989;6:133–9. https://doi.org/10.1023/a:1015928509 101.
- Sandra L, Smits A, Allegaert K, Nicolaï J, Annaert P, Bouillon T. Population pharmacokinetics of propofol in neonates and infants: gestational and postnatal age to determine clearance maturation. Br J Clin Pharmacol. 2021;87(4):2089–97. https://doi.org/10. 1111/bcp.14620.
- D'Argenio DZ, Schumitzky A, Wang X. ADAPT 5 user's guide: pharmacokinetic/pharmacodynamic systems analysis software. Los Angeles: Biomedical Simulations Resource; 2009. p. 1–316.

- Rossi M, Oliveira J, Zucoloto S, Pissaia O, Costa R. Effect of protein-calorie malnutrition on catecholamine levels and weight of heart in rats. J Neural Transm. 1980;48:85–99. https://doi.org/ 10.1007/BF01250038.
- Blake CM, Kharasch E, Schwab M, Nagele P. A meta-analysis of CYP2D6 metabolizer phenotype and metoprolol pharmacokinetics. CPT. 2013;94(3):394–9. https://doi.org/10.1038/clpt.2013.96.
- Funai Y, Takemura M, Inoue K, Shirasaka Y. Effect of ingested fluid volume and solution osmolality on intestinal drug absorption: Impact on drug interaction with beverages. Eur J Pharm Sci. 2022;172: 106136. https://doi.org/10.1016/j.ejps.2022.106136.
- Sjögren E, Tarning J, Barnes KI, Jonsson EN. A physiologicallybased pharmacokinetic framework for prediction of drug exposure in malnourished children. Pharmaceutics. 2021;13(2):204. https:// doi.org/10.3390/pharmaceutics13020204.
- Vinarov Z, Abdallah M, Agundez JA, Allegaert K, Basit AW, Braeckmans M, et al. Impact of gastrointestinal tract variability on oral drug absorption and pharmacokinetics: an UNGAP review. Eur J Pharm Sci. 2021;162: 105812. https://doi.org/10.1016/j.ejps. 2021.105812.
- Dressman J, Fleisher D. Mixing-tank model for predicting dissolution rate control of oral absorption. J Pharm Sci. 1986;75(2):109–16. https://doi.org/10.1002/jps.2600750202.
- Macheras P, Chryssafidis P. Revising pharmacokinetics of oral drug absorption: I models based on biopharmaceutical/physiological and finite absorption time concepts. Pharm Res. 2020;37:1–13. https://doi.org/10.1007/s11095-020-02894-w.

Authors and Affiliations

Fatma Kir^{1,2} · Selma Sahin¹ · William J. Jusko²

- William J. Jusko wjjusko@buffalo.edu
- Department of Pharmaceutical Technology, Faculty of Pharmacy, Hacettepe University, 06100 Ankara, Turkey
- Department of Pharmaceutical Sciences, School of Pharmacy and Pharmaceutical Sciences, State University of New York at Buffalo, 404 Pharmacy Building, Buffalo, NY 14214-8033, USA